CHEMISTRY OF MATERIALS
Cite This: Chem. Mater. XXXX, XXX, XXX–XXX
Article
pubs.acs.org/cm

All Roads Lead to TiO_2: TiO_2-Rich Surfaces of Barium and Strontium Titanate Prepared by Hydrothermal Synthesis

Lawrence A. Crosby,[†] Bor-Rong Chen,[†] Robert M. Kennedy,[‡] Jianguo Wen,[§] Kenneth R. Poeppelmeier,[‡] Michael J. Bedzyk,[†] and Laurence D. Marks*[,†]

[†]Department of Materials Science and Engineering, Northwestern University, Evanston, Illinois 60208, United States
[‡]Department of Chemistry, Northwestern University, Evanston, Illinois 60208, United States
[§]Center for Nanoscale Materials, Argonne National Laboratory, Lemont, Illinois 60439, United States

Supporting Information

ABSTRACT: Through high-resolution electron microscopy, the surface structure of barium titanate and strontium titanate nanoparticles are found to be terminated by a TiO_2 double layer. These results confirm prior observations of TiO_2-rich surface reconstructions on strontium titanate nanoparticles made hydrothermally at high pH and single crystals prepared with wet chemical etching. Of all the reconstructions observed on single crystals for these two materials, we report for first time the $\sqrt{13} \times \sqrt{13}R33.7°$ structure on the {001} facets of hydrothermally prepared barium titanate and strontium titanate nanocrystals. The aqueous environment common to the two preparation methods preferentially leaves strontium and barium depleted from the A-sites near the surface and leads to TiO_2-terminated surfaces for both materials. Analysis indicates that the observed structures are the thermodynamic lowest energy structures in aqueous conditions.

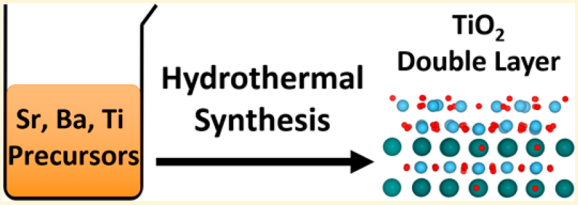

INTRODUCTION

Nanoparticles with well-controlled shapes and sizes are highly desirable and are often sought as the end goal of nanoparticle synthesis because regular shape and size can be exploited for applications. At the nanoscale, materials properties can, and often do, deviate from those of their bulk counterparts. Strontium titanate (STO) and barium titanate (BTO) are two materials of importance that have been well-studied at both the mesoscale and the nanoscale. The surface of STO has been particularly well-studied, with many reports in the literature.[1−8] BTO has also been widely studied due to its ferroelectric properties and phase transitions at the nanoscale.[9−14] Developing further applications for such materials will require understanding of which properties deviate from the bulk and under what conditions.

While the overall shape of many oxide nanoparticles as a function of hydrothermal synthesis conditions is now established, the surface structure is known in only a few rare cases. For many applications, the surfaces are more important than the bulk, for instance when oxide nanoparticles are used as supports in heterogeneous catalysis. A few examples from recent literature show that properties such as conductivity and photocatalytic activity are facet-dependent,[15,16] and ferroelectric properties have the potential to affect catalysis in operando.[17] It is established that the surface of STO at the macroscale can be very complex,[18−20] but whether this carries over to nanoparticles is unknown.

Here, we report several atomically resolved surfaces observed using high resolution electron microscopy (HREM) on BTO and STO nanoparticles. We find that the surfactant molecules influence the nanoparticle faceting but that the aqueous environment favors TiO_2-rich surface chemistry. The {001} surfaces all have experimental contrast that matches the same surface reconstruction reported in work on single crystals.

METHODS

The solvothermal synthesis of STO developed by Rabuffetti et al.[21] was modified to study the effects of substitution of different organic acids. STO nanocuboids were prepared using caprylic (octanoic) acid (STO-CA) as the surfactant. Equivalent molar concentrations of titanium tetrabutoxide ($Ti(OBu)_4$) and strontium acetate ($Sr(Ac)_2$) were used in place of the reagents in the previously published method, and the temperature was reduced to 180 °C (see Table 1).

BTO nanocuboids were prepared by substituting barium hydroxide octahydrate ($Ba(OH)_2{\cdot}8H_2O$) for strontium hydroxide octahydrate ($Sr(OH)_2{\cdot}8H_2O$) in the method of Rabuffetti et al. while doubling the precursor concentration with equimolar proportions. The reaction temperature for BTO was also reduced from 240 to 180 °C (see Table 1).

STO dodecahedra were prepared using glycerol (STO-G) as the surfactant; the details of the preparation appear elsewhere.[22,23] Note that the surfactants were removed by sonicating and centrifuging the samples repeatedly in ethanol (STO-G) or deionized water (BTO, STO-CA).

For transmission electron microscopy (TEM) imaging, the samples were dispersed in ethanol and drop-casted onto lacey carbon TEM

Received: October 19, 2017
Revised: January 18, 2018
Published: January 18, 2018

DOI: 10.1021/acs.chemmater.7b04404
Chem. Mater. XXXX, XXX, XXX–XXX

Table 1. Table for Synthesis Parameters for Solvothermal Synthesis of BTO and STO, as Discussed in This Article[a]

A site precursor	B site precursor	T (°C)	surfactant	pK_a	primary faceting	surface chemistry	article
$Sr(OH)_2{\cdot}8H_2O$	$TiCl_4$	240	acetic acid	4.74	{001}	TiO_2	Lin et al.[26]
$Ba(OH)_2{\cdot}8H_2O$	$TiCl_4$	180	acetic acid	4.74	{001}	TiO_2	this work
$Sr(Ac)_2$	$Ti(OBu)_4$	180	caprylic acid	4.89	{001}	TiO_2	this work
$Sr(Ac)_2$	$Ti(OBu)_4$	180	oleic acid	9.85	{001}	SrO	Lin et al.[26] Hu et al.[27]
$Sr(Ac)_2$	$Ti(OBu)_4$	240	glycerol	14.1	{110} and minority {001}	TiO_2	Crosby et al.[23] this work

[a]Note that only one case (with oleic acid as surfactant) results in A-site-rich surface terminations.

grids. All imaging was performed using the Argonne chromatic aberration-corrected TEM (ACAT) operating at 200 kV.

To identify the surface structure, several model surface structures (see Supporting Information) were used to simulate TEM images using the MacTempas software program. All CIF structures used as input for simulations have been previously reported,[24,25] with the exception of bulk AO and TiO_2 supercells, which appear in the Supporting Information. Microscope simulation parameters were spherical aberration coefficient C_s = −0.0050 mm, defocal spread due to chromatic aberration Δf = 30 Å, convergence angle α = 0.5 mrad, C_{s5} = 0, and coma = 0. The thickness was varied to fit the experimental images, paying attention to geometric constraints imposed by the shape of the nanoparticles. The defocus was also varied to obtain a good fit to the bulk so that the agreement with the surface was an unbiased result.

RESULTS

The solvothermal syntheses resulted in nanoparticles with a range of mean particle sizes (distance between parallel facets): 100 nm for BTO (Figure 1a), 140 nm for STO-G (Figure 1b), and 80 nm for STO-CA (Figure 1c). The particles ranged in size from 50 to 130 nm for BTO case, 20−200 nm for STO-G, and 40 nm to 80 nm for STO-CA.

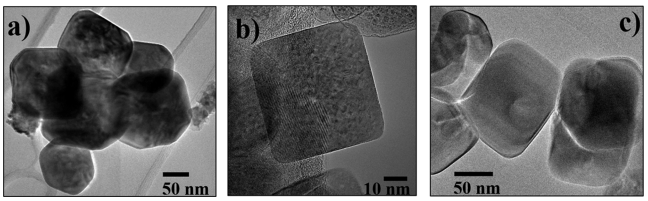

Figure 1. Low resolution TEM images of (a) BTO, (b) STO-G, and (c) STO-CA.

The particles synthesized using organic acid surfactants (BTO and STO-CA) resulted in cuboidal shapes which are predominantly {001} terminated with rounded corners. The STO-G synthesis resulted in rhombic dodecahedra, which are predominantly {110} terminated. (We note that there is minor faceting of {001} present for these particles as well; see Table 1.)

High resolution electron microscopy revealed the surface morphology of the three different preparations, as described in the Methods section. All particle surfaces were imaged using profile view imaging,[28,29] which is sensitive to atomic number for thin samples. For the {001} facets, the best match was obtained using the $\sqrt{13} \times \sqrt{13}$ $R33.7°$ reconstruction (see Figure 2) as shown for STO-G (Figure 3), STO-CA (Figure 4), and BTO samples (Figure 5). This structure has a TiO_2 double-layer (DL) at the surface and has previously been observed on STO nanocuboids prepared using acetic acid, as well as single crystals.[24,26,30] There is also a small region (see Figure 3, Region 1) that corresponds to a triple layer structure, which matches reasonably well to anatase titania [001] for the extra half unit cell (see Figure 3). This agrees with the observed epitaxial growth of anatase titania on STO single crystals.[31]

Measurements of the d-spacings of the surface and subsurface layer were 2.1 Å for the experimental image as depicted in Figure 5c and 2.3 Å for the simulation shown in Figure 5d. This is a deviation of approximately 10%, which is comparable with the difference in the atomic radii between Ba and Sr. Given that the BTO RT13 simulation supercell was constructed by adapting the solved STO structure[24] cells and substituting the Sr atoms with Ba, this is quite good agreement between the simulated and experimental contrast.

Simulated HREM for other possible surface structures, including the 3×3 and $\sqrt{5} \times \sqrt{5}$ as reported in previous work by Kienzle et al.[24] as well as the c(6×2) structure reported in work by Ciston et al.,[25] appear in the Supporting Information (see Figures S3−S7). None of the alternatives were an adequate match to the experimental results. Comparable analysis for the {110} facets of STO-G can be found in Supporting Information of previous work.[23]

DISCUSSION

The results for both the {001} and the {110} indicate that TiO_2-rich surfaces are very common and are likely pervasive for hydrothermal synthesis. There is also literature that reports stable epitaxial growth of anatase titania on STO single crystals.[31] It is well-known that acid etching preparation of bulk single crystal STO produces TiO_2-rich surfaces.[32−35] In fact, there are several reports of deionized water etching STO to obtain TiO_2-terminated surfaces.[36,37] In these cases, the pH was in the acidic range (below 7), which preferentially etches SrO, a basic oxide.

In our case, the pH of the solution is significantly higher (∼14) during the growth phase of the nanoparticle synthesis. Alkaline conditions are required to stabilize the formation of crystalline BTO and STO.[38] Comparing the nanoparticle growth conditions with the etching conditions reported for single crystal studies, the presence of surfactants is a key difference between the two. Thus, for our case, the surfactants will play a key role in determining the final surface chemistry of the nanoparticles.

It is well-known that surfactant molecules can significantly change the shape of nanoparticles through preferential adsorption during the growth process. Several surfactants were investigated in this study. Acetic acid and caprylic acid are both carboxylates with the same functional group. Glycerol is a multidentate polyol with a very different molecular structure. Large differences in acidity can be seen by the wide range pK_a values in Table 1. Despite these differences, all syntheses yielded titania-rich surfaces. A discussion of stabilization of

DOI: 10.1021/acs.chemmater.7b04404
Chem. Mater. XXXX, XXX, XXX−XXX

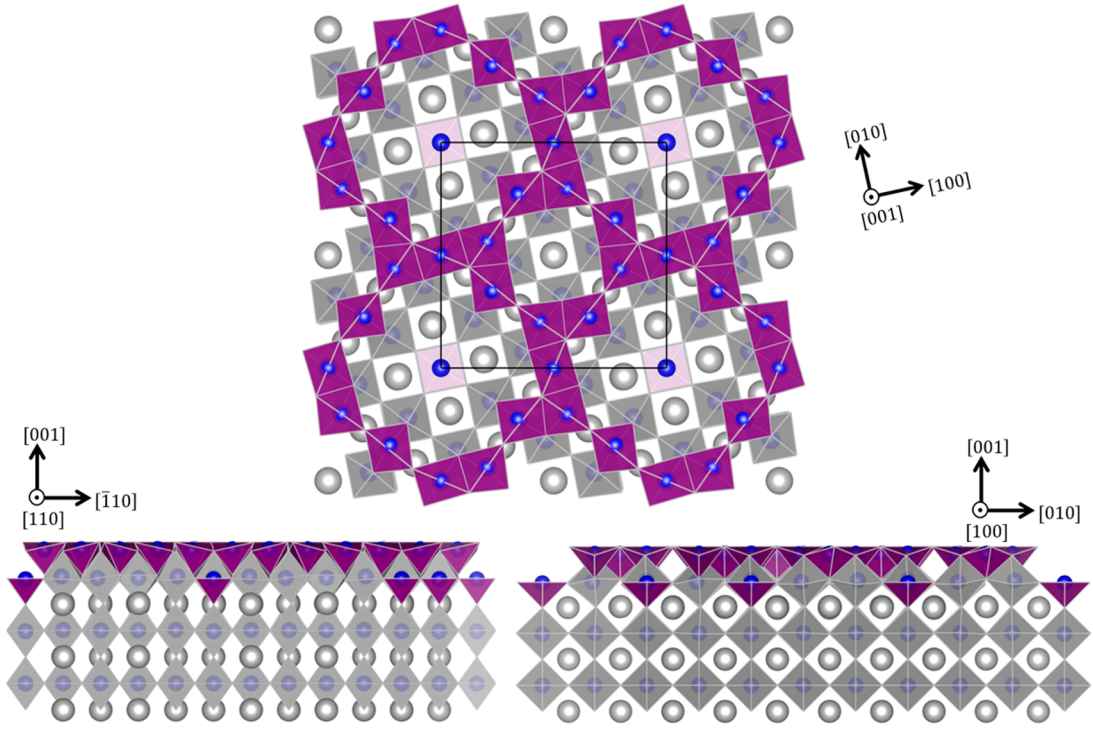

Figure 2. Polyhedral model of a 2 × 2 supercell of the RT13 reconstruction as reported in ref 24 viewed top-down and side-on. Note that the purple surface units correspond to TiO_5 truncated octahedra.

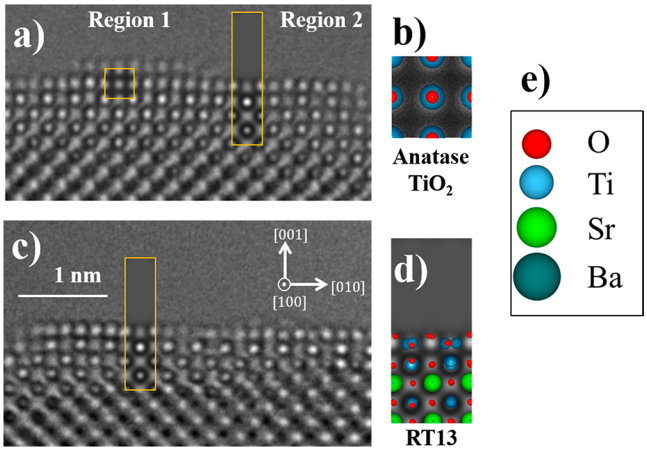

Figure 3. (a) Experimental image of STO-G (001) surface imaged along the [100] zone axis, with simulated image insets of anatase titania [001] (region 1) and the RT13 reconstruction (region 2). (b) Atomic structure of anatase TiO_2 unit cell along the [001] zone axis. (c) Second experimental image of STO-G (001) surface along the [100] zone, with simulation of STO RT13 inset. (d) Atomic structure of the STO RT13 reconstruction viewed along the [100] zone axis. (e) Key for colors corresponding to O, Ti, Sr, and Ba used in atomic models. Note that the simulations correspond to a single bulk unit cell (orange box) along the projected direction. The conditions for all simulations were: thickness = 39 Å, focus = 40 Å, and crystal tilt = 0.

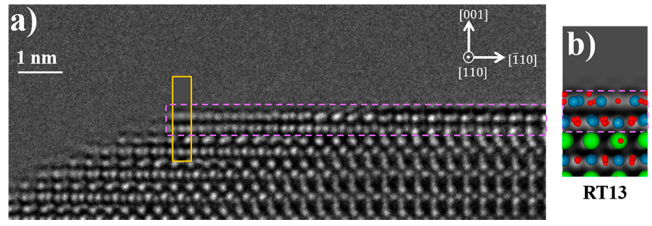

Figure 4. (a) Experimental image of STO-CA particle (001) surface imaged along the [110] zone axis, with simulated image inset of the STO RT13 reconstruction. (b) Atomic structure of the STO RT13. Note that the simulation corresponds to a single bulk unit cell (orange box) along the projected direction. The simulation conditions were: thickness = 84 Å, focus = 40 Å, and crystal tilt 7 mrad with an azimuthal angle of 45°. Note contrast matching a TiO_2 double layer at the surface (the surface and subsurface layers are highlighted with dashed purple rectangles).

alkali and alkaline earth metal ions by various ligands can be found in work by Daniele et al.[39] The instability of such ionic complexes with alcohol compared with carboxylates can inform the observation of titania-rich {110} surfaces as reported in previous work[23] and {001} surfaces in this study.

In studies on single crystals, SrO_x surfaces are obtained by annealing at high temperatures in oxygen-rich environments.[40−43] Water is known to react with SrO to form $Sr(OH)_2$.[44] The case of BaO is similar;[45] like SrO,[46] it will readily form a hydroxide, which will not revert to the oxide unless heated in an inert atmosphere to temperatures between 530 and 600 °C. Thus, it is important to prevent A-site terminated surfaces from being etched by water.

To date, the only nanoparticle syntheses of which the authors are aware that results in A-site terminated surfaces involve the use of liquid microemulsions.[27,47] For the purposes of this study, the molecular structure is the important factor to determine the surface chemistry; see differences in Figure 6. With sufficient packing density of the surfactant[48] and a sufficiently long hydrocarbon tail, the surfaces should be protected from being etched by water in the solution via steric hindrance. By targeting a water-poor region of the water/oil/alcohol phase diagram in which lamellar liquid crystals form, SrO-terminated nanocrystals were obtained using oleic acid.[26] We suspect other reports in the literature using similar reaction

DOI: 10.1021/acs.chemmater.7b04404
Chem. Mater. XXXX, XXX, XXX−XXX

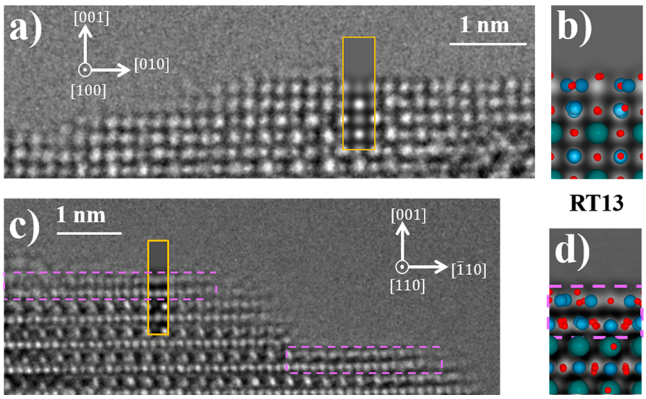

Figure 5. (a) Experimental image of BTO particle (001) surface imaged along the [100] zone axis and with simulated images of the BTO RT13 reconstruction inset. (b) Atomic structure of BTO RT13 along the [100] zone axis. (c) Experimental image of BTO particle (001) surface along the [110] zone axis, with simulated image contrast of the BTO RT13 reconstruction inset. (d) Atomic structure of the BTO RT13 along the [110] zone axis. The simulations correspond to a single bulk unit cell (red box) along the projected direction. The conditions for all simulations were: thickness = 84 Å, focus = 50 Å, and crystal tilt 7 mrad with an azimuthal angle of −45°. Note contrast matching a TiO_2 double layer at the surface terraces (the surface and subsurface layers are highlighted with dashed purple rectangles).

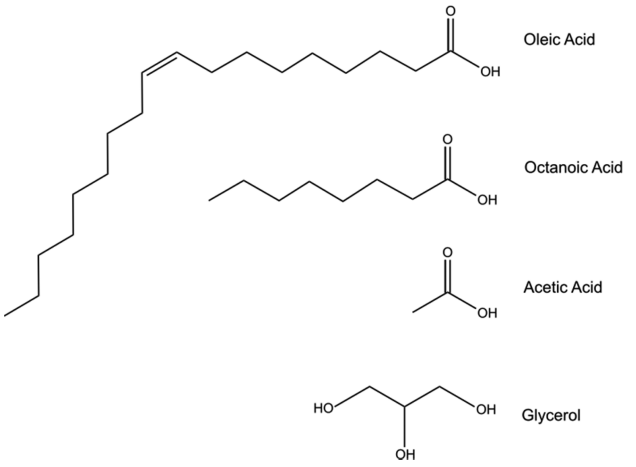

Figure 6. Molecular structure of various surfactants used in hydrothermal synthesis of titanates. All except oleic acid are used in this study.

conditions are also A-site terminated, although characterization to determine this is not reported.[49,50]

Turning now to the specific surface structure, the RT13 surface structure was observed for all materials discussed in this article, independent of the choice of organic acid or glycerol, with the exception of oleic acid (see work by Lin et al.[26]). The RT13 surface reconstruction is one of the low energy structures, as evidenced by the convex hull construction shown in Figure 7. It was first produced and solved for flat surfaces by treating large single crystals using buffered etching conditions and annealed in oxidizing environments. It has since been observed for many other cases with the (001) surface of STO[30,34] and has been reported in one paper for BTO.[51] To understand more specifically the thermodynamics, we need to combine the energies as a function of the excess of TiO_2 from Figure 7 with the reactions:

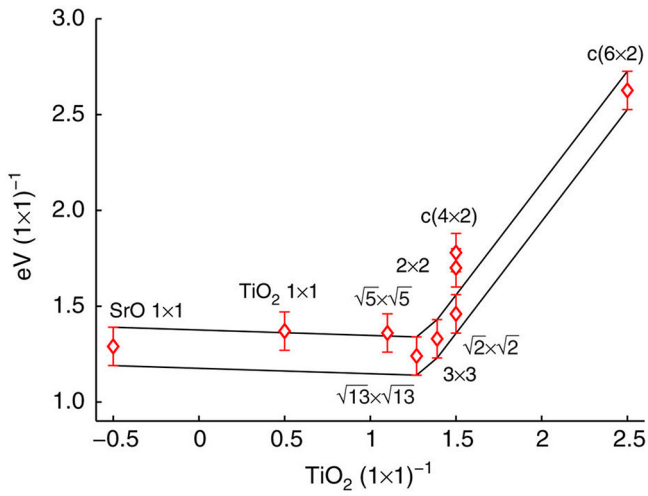

Figure 7. Surface enthalpies versus excess TiO_2 at the surface, calculated from DFT known reconstructions on strontium titanate {001} surfaces. The energies are referenced to bulk STO and anatase TiO_2. Reproduced with permission from ref 25.

$$SrTiO_3(bulk) \rightleftharpoons SrO(bulk) + TiO_2(bulk) \quad (1)$$

$$SrO(bulk) + H_2O(aq) \rightleftharpoons Sr(OH)_2(aq) \quad (2)$$

Relevant numbers are given in Table 2.

Table 2. Standard Enthalpies of Formation for Species Involved in STO Surface Chemistry

species	ΔH_f^o (kJ/mol)	ΔH_f^o (eV/1 × 1)	ref
$SrTiO_3$ (bulk)	−1590	−16.5	Lencka and Riman[52]
SrO (bulk)	−551	−5.71	Lencka and Riman[52]
$Sr(OH)_2$(aq)	−1010	−10.5	Lencka and Riman[52]
TiO_2 (bulk)	−946	−9.84	Lencka and Riman[38]
H_2O	−286	−2.96	JANAF Tables[53]
TiO_2 (surface SL)		1.40	Figure 7
TiO_2 (surface DL)		1.30	Figure 7

The enthalpy of reaction 1 is 49.3 kJ/mol or 0.51 eV/(1 × 1) and reaction 2 is −93.7 kJ/mol or −0.97 eV/(1 × 1). Hence, the reduction in energy per surface excess of TiO_2 will be given by approximately 1 eV per unit cell for each additional surface (1 × 1) with an increase in energy equivalent to the surface energy values given in Figure 7. The SrO surface termination is similar in energy to the TiO_2-rich structures along the convex hull, but the hydrolysis favors dissolution of this surface in solution via reaction 2. From the numbers, further increasing the coverage of TiO_2 beyond that of the RT13 will result in an increase in surface energy that overwhelms the hydrolysis reaction. The universal observation of titania-rich surfaces, in particular the occurrence of the RT13, can thus be explained as the formation of the global thermodynamic lowest energy surface structure in aqueous conditions.

CONCLUSIONS

We demonstrated that hydrothermal routes to synthesize titanate nanomaterials generally result in TiO_2 terminated surfaces. These surfaces are stable as 4- and 5-coordinated polyhedra, as confirmed by HREM. While TiO_6 octahedra are preferred, truncated octahedral TiO_5 units[24] form the frame-

DOI: 10.1021/acs.chemmater.7b04404
Chem. Mater. XXXX, XXX, XXX−XXX

work of the RT13 reconstruction observed on STO (001), and TiO_4 tetrahedra are the building blocks of the ($n \times 1$) homologous series of reconstructions[8,54] observed on the STO (110) surface. The driving force for the formation of the TiO_2-rich surfaces is thermodynamics in aqueous conditions.

■ ASSOCIATED CONTENT

Supporting Information

The Supporting Information is available free of charge on the ACS Publications website at DOI: 10.1021/acs.chemmater.7b04404.

Detailed discussion of multislice simulations (PDF)

CIF structures for bulk crystal truncations used in simulations (ZIP)

■ AUTHOR INFORMATION

Corresponding Author

*E-mail: l-marks@northwestern.edu.

ORCID

Lawrence A. Crosby: 0000-0001-7644-3762

Robert M. Kennedy: 0000-0001-6836-7923

Kenneth R. Poeppelmeier: 0000-0003-1655-9127

Michael J. Bedzyk: 0000-0002-1026-4558

Notes

The authors declare no competing financial interest.

■ ACKNOWLEDGMENTS

This material is based upon work supported by the U.S. Department of Energy, Office of Science, Office of Basic Energy Sciences under Award DOE DE-FG02-03-ER154757. L.C. also acknowledges support from a National Science Foundation Graduate Fellowship. Use of aberration-corrected TEM at the Center for Nanoscale Materials, an Office of Science user facility, supported by the U.S. Department of Energy, Office of Science, Office of Basic Energy Sciences, under Contract DE-AC02-06CH11357 is acknowledged.

■ REFERENCES

(1) Jiang, Q. D.; Zegenhagen, J. c(6 × 2) and c(4 × 2) Reconstruction of $SrTiO_3$ (001). *Surf. Sci.* **1999**, *425*, 343−354.

(2) Erdman, N.; Poeppelmeier, K. R.; Asta, M.; Warschkow, O.; Ellis, D. E.; Marks, L. D. The Structure and Chemistry of the TiO_2-Rich Surface of $SrTiO_3$ (001). *Nature* **2002**, *419*, 55−58.

(3) Erdman, N.; Warschkow, O.; Asta, M.; Poeppelmeier, K. R.; Ellis, D. E.; Marks, L. D. Surface Structures of $SrTiO_3$ (001): A TiO_2-Rich Reconstruction with a c(4 × 2) Unit Cell. *J. Am. Chem. Soc.* **2003**, *125*, 10050−10056.

(4) Deak, D. S.; Silly, F.; Newell, D. T.; Castell, M. R. Ordering of TiO_2-Based Nanostructures on $SrTiO_3$ (001) Surfaces. *J. Phys. Chem. B* **2006**, *110*, 9246−9251.

(5) Silly, F.; Newell, D. T.; Castell, M. R. $SrTiO_3$ (001) Reconstructions: The (2 × 2) to c(4 × 4) Transition. *Surf. Sci.* **2006**, *600*, L219−L223.

(6) Heifets, E.; Piskunov, S.; Kotomin, E. A.; Zhukovskii, Y. F.; Ellis, D. E. Electronic Structure and Thermodynamic Stability of Double-Layered $SrTiO_3$ (001) Surfaces: Ab Initio Simulations. *Phys. Rev. B: Condens. Matter Mater. Phys.* **2007**, *75*, 115417.

(7) Wohlwend, J. L.; Behera, R. K.; Jang, I.; Phillpot, S. R.; Sinnott, S. B. Morphology and Growth Modes of Metal-Oxides Deposited on $SrTiO_3$. *Surf. Sci.* **2009**, *603*, 873−880.

(8) Wang, Z.; Loon, A.; Subramanian, A.; Gerhold, S.; McDermott, E.; Enterkin, J. A.; Hieckel, M.; Russell, B. C.; Green, R. J.; Moewes, A.; Guo, J.; Blaha, P.; Castell, M. R.; Diebold, U.; Marks, L. D. Transition from Reconstruction Toward Thin Film on the (110) Surface of Strontium Titanate. *Nano Lett.* **2016**, *16*, 2407−2412.

(9) Haertling, G. H. Ferroelectric Ceramics: History and Technology. *J. Am. Ceram. Soc.* **1999**, *82*, 797−818.

(10) Damjanovic, D. Ferroelectric, Dielectric and Piezoelectric Properties of Ferroelectric Thin Films and Ceramics. *Rep. Prog. Phys.* **1998**, *61*, 1267−1324.

(11) Shih, W. Y.; Shih, W.-H.; Aksay, I. A. Size Dependence of the Ferroelectric Transition of Small $BaTiO_3$ Particles: Effect of Depolarization. *Phys. Rev. B: Condens. Matter Mater. Phys.* **1994**, *50*, 15575−15585.

(12) Frey, M. H.; Payne, D. A. Grain-Size Effect on Structure and Phase Transformations for Barium Titanate. *Phys. Rev. B: Condens. Matter Mater. Phys.* **1996**, *54*, 3158−3168.

(13) Smith, M. B.; Page, K.; Siegrist, T.; Redmond, P. L.; Walter, E. C.; Seshadri, R.; Brus, L. E.; Steigerwald, M. L. Crystal Structure and the Paraelectric-to-Ferroelectric Phase Transition of Nanoscale $BaTiO_3$. *J. Am. Chem. Soc.* **2008**, *130*, 6955−6963.

(14) Park, Y.; Lee, W.-J.; Kim, H.-G. Particle-Size-Induced Diffuse Phase Transition in the Fine-Particle Barium Titanate Porcelains. *J. Phys.: Condens. Matter* **1997**, *9*, 9445−9456.

(15) Tan, C.-S.; Hsu, S.-C.; Ke, W.-H.; Chen, L.-J.; Huang, M. H. Facet-Dependent Electrical Conductivity Properties of Cu2o Crystals. *Nano Lett.* **2015**, *15*, 2155−2160.

(16) Li, J.; Bai, H.; Yi, W.; Liu, J.; Li, Y.; Zhang, Q.; Yang, H.; Xi, G. Synthesis and Facet-Dependent Photocatalytic Activity of Strontium Titanate Polyhedron Nanocrystals. *Nano Res.* **2016**, *9*, 1523−1531.

(17) Kakekhani, A.; Ismail-Beigi, S. Ferroelectric-Based Catalysis: Switchable Surface Chemistry. *ACS Catal.* **2015**, *5*, 4537−4545.

(18) Castell, M. R. Scanning Tunneling Microscopy of Reconstructions on the $SrTiO_3$(001) Surface. *Surf. Sci.* **2002**, *505*, 1−13.

(19) Zhu, G.-z.; Radtke, G.; Botton, G. A. Bonding and Structure of a Reconstructed (001) Surface of $SrTiO_3$ from TEM. *Nature* **2012**, *490*, 384−387.

(20) Marshall, M. S. J.; Becerra-Toledo, A. E.; Marks, L. D.; Castell, M. R. Defects on Strontium Titanate. In *Defects at Oxide Surfaces*; Springer Series in Surface Sciences: Springer, Cham, 2015; pp 327−349.

(21) Rabuffetti, F. A.; Kim, H. S.; Enterkin, J. A.; Wang, Y. M.; Lanier, C. H.; Marks, L. D.; Poeppelmeier, K. R.; Stair, P. C. Synthesis-Dependent First-Order Raman Scattering in $SrTiO_3$ Nanocubes at Room Temperature. *Chem. Mater.* **2008**, *20*, 5628−5635.

(22) Dong, L. Q.; Shi, H.; Cheng, K.; Wang, Q.; Weng, W. J.; Han, W. Q. Shape-Controlled Growth of $SrTiO_3$ Polyhedral Submicro/Nanocrystals. *Nano Res.* **2014**, *7*, 1311−1318.

(23) Crosby, L. A.; Kennedy, R. M.; Chen, B.-R.; Wen, J.; Poeppelmeier, K. R.; Bedzyk, M. J.; Marks, L. D. Complex Surface Structure of (110) Terminated Strontium Titanate Nanododecahedra. *Nanoscale* **2016**, *8*, 16606−16611.

(24) Kienzle, D. M.; Becerra-Toledo, A. E.; Marks, L. D. Vacant-Site Octahedral Tilings on $SrTiO_3$ (001), the ($\sqrt{13} \times \sqrt{13}$)R33.7° Surface, and Related Structures. *Phys. Rev. Lett.* **2011**, *106*, 176102.

(25) Ciston, J.; Brown, H. G.; D'Alfonso, A. J.; Koirala, P.; Ophus, C.; Lin, Y.; Suzuki, Y.; Inada, H.; Zhu, Y.; Allen, L. J.; Marks, L. D. Surface Determination Through Atomically Resolved Secondary-Electron Imaging. *Nat. Commun.* **2015**, *6*, 7358.

(26) Lin, Y.; Wen, J.; Hu, L.; Kennedy, R. M.; Stair, P. C.; Poeppelmeier, K. R.; Marks, L. D. Synthesis-Dependent Atomic Surface Structures of Oxide Nanoparticles. *Phys. Rev. Lett.* **2013**, *111* (15), 156101.

(27) Hu, L.; Wang, C.; Kennedy, R. M.; Marks, L. D.; Poeppelmeier, K. R. The Role of Oleic Acid: From Synthesis to Assembly of Perovskite Nanocuboid Two-Dimensional Arrays. *Inorg. Chem.* **2015**, *54*, 740−745.

(28) Marks, L. D. Direct Imaging of Carbon-Covered and Clean Gold (110) Surfaces. *Phys. Rev. Lett.* **1983**, *51*, 1000−1002.

(29) Marks, L. D.; Smith, D. J. Direct Surface Imaging in Small Metal Particles. *Nature* **1983**, *303*, 316.

DOI: 10.1021/acs.chemmater.7b04404
Chem. Mater. XXXX, XXX, XXX−XXX

(30) Shimizu, R.; Ohsawa, T.; Iwaya, K.; Shiraki, S.; Hitosugi, T. Epitaxial Growth Process of $La_{0.7}Ca_{0.3}MnO_3$ Thin Films on $SrTiO_3$ (001): Thickness-Dependent Inhomogeneity Caused by Excess Ti Atoms. *Cryst. Growth Des.* **2014**, *14*, 1555−1560.
(31) Saitoh, H.; Sunayama, H.; Tanaka, N.; Ohshio, S. Epitaxial Growth Mechanism of Chemical-Vapor-Deposited Anatase on Strontium Titanate Substrate. *Nippon Seramikkusu Kyokai Gakujutsu Ronbunshi* **1998**, *106*, 1051−1055.
(32) Koster, G.; Kropman, B. L.; Rijnders, G. J. H. M.; Blank, D. H. A.; Rogalla, H. Quasi-Ideal Strontium Titanate Crystal Surfaces Through Formation of Strontium Hydroxide. *Appl. Phys. Lett.* **1998**, *73*, 2920−2922.
(33) Kawasaki, M.; Takahashi, K.; Maeda, T.; Tsuchiya, R.; Shinohara, M.; Ishiyama, O.; Yonezawa, T.; Yoshimoto, M.; Koinuma, H. Atomic Control of the $SrTiO_3$ Crystal Surface. *Science* **1994**, *266*, 1540−1542.
(34) Biswas, A.; Rossen, P. B.; Yang, C.-H.; Siemons, W.; Jung, M.-H.; Yang, I. K.; Ramesh, R.; Jeong, Y. H. Universal Ti-Rich Termination of Atomically Flat $SrTiO_3$ (001), (110), and (111) Surfaces. *Appl. Phys. Lett.* **2011**, *98*, 051904.
(35) Wang, C.; Koirala, P.; Stair, P.; Marks, L. ALD Synthesis of Platinum Nanoparticles on Single-Crystal $SrTiO_3$ Pretreated with Wet Chemical Etching. *Appl. Surf. Sci.* **2017**, *422*, 661−665.
(36) Hatch, R. C.; Fredrickson, K. D.; Choi, M.; Lin, C.; Seo, H.; Posadas, A. B.; Demkov, A. A. Surface Electronic Structure for Various Surface Preparations of Nb-Doped $SrTiO_3$ (001). *J. Appl. Phys.* **2013**, *114*, 103710.
(37) Hatch, R. C.; Choi, M.; Posadas, A. B.; Demkov, A. A. Comparison of Acid- and Non-Acid-Based Surface Preparations of Nb-Doped $SrTiO_3$ (001). *J. Vac. Sci. Technol., B: Nanotechnol. Microelectron.: Mater., Process., Meas., Phenom.* **2015**, *33*, 061204.
(38) Lencka, M. M.; Riman, R. E. Thermodynamics of the Hydrothermal Synthesis of Calcium Titanate with Reference to Other Alkaline-Earth Titanates. *Chem. Mater.* **1995**, *7*, 18−25.
(39) Daniele, P. G.; Foti, C.; Gianguzza, A.; Prenesti, E.; Sammartano, S. Weak Alkali and Alkaline Earth Metal Complexes of Low Molecular Weight Ligands in Aqueous Solution. *Coord. Chem. Rev.* **2008**, *252*, 1093−1107.
(40) Meyer, R.; Waser, R.; Helmbold, J.; Borchardt, G. Cationic Surface Segregation in Donor-Doped $SrTiO_3$ Under Oxidizing Conditions. *J. Electroceram.* **2002**, *9*, 101−110.
(41) Bachelet, R.; Sánchez, F.; Palomares, F. J.; Ocal, C.; Fontcuberta, J. Atomically Flat SrO-Terminated $SrTiO_3$ (001) Substrate. *Appl. Phys. Lett.* **2009**, *95*, 141915.
(42) Schrott, A. G.; Misewich, J. A.; Copel, M.; Abraham, D. W.; Zhang, Y. A-Site Surface Termination in Strontium Titanate Single Crystals. *Appl. Phys. Lett.* **2001**, *79*, 1786−1788.
(43) Nishimura, J.; Ohtomo, A.; Ohkubo, A.; Murakami, Y.; Kawasaki, M. Controlled Carrier Generation at a Polarity-Discontinued Perovskite Heterointerface. *Jpn. J. Appl. Phys.* **2004**, *43*, L1032−L1034.
(44) Patnaik, P. *Handbook of Inorganic Chemicals*; McGraw-Hill: New York, 2003.
(45) Habashy, G. M.; Kolta, G. A. Thermal Decomposition of the Hydrates of Barium Hydroxide. *J. Inorg. Nucl. Chem.* **1972**, *34*, 57−67.
(46) Dinescu, R.; Preda, M. Thermal Decomposition of Strontium Hydroxide. *J. Therm. Anal.* **1973**, *5*, 465−473.
(47) Hu, L. H.; Wang, C. D.; Lee, S.; Winans, R. E.; Marks, L. D.; Poeppelmeier, K. R. $SrTiO_3$ Nanocuboids from a Lamellar Microemulsion. *Chem. Mater.* **2013**, *25*, 378−384.
(48) Wood, M. H.; Casford, M. T.; Steitz, R.; Zarbakhsh, A.; Welbourn, R. J. L.; Clarke, S. M. Comparative Adsorption of Saturated and Unsaturated Fatty Acids at the Iron Oxide/Oil Interface. *Langmuir* **2016**, *32*, 534−540.
(49) Cai, W.; Rao, T.; Wang, A.; Hu, J.; Wang, J.; Zhong, J.; Xiang, W. A Simple and Controllable Hydrothermal Route for the Synthesis of Monodispersed Cube-Like Barium Titanate Nanocrystals. *Ceram. Int.* **2015**, *41*, 4514−4522.
(50) Xiaowei, Y.; Yanwei, Z.; Leiqing, M.; Longxiang, H. Oleic Acid Assisted Glycothermal Synthesis of Cuboidal $Ba_{0.6}Sr_{0.4}TiO_3$ Nanocrystals and Their Ordered Architectures via Self-Assembly. *J. Colloid Interface Sci.* **2011**, *357*, 308−316.
(51) Morales, E. H.; Bonnell, D. A. On the Relationship Between Surface Reconstructions and Step Edge Stability on $BaTiO_3$ (001). *Surf. Sci.* **2013**, *609* (Supplement C), 62−66.
(52) Lencka, M. M.; Riman, R. E. Hydrothermal Synthesis of Perovskite Materials: Thermodynamic Modeling and Experimental Verification. *Ferroelectrics* **1994**, *151*, 159−164.
(53) Water, 10 bar (H_2O). NIST-JANAF thermochemical tables http://kinetics.nist.gov/janaf/html/H-066.html (accessed October 3, 2017).
(54) Enterkin, J. A.; Subramanian, A. K.; Russell, B. C.; Castell, M. R.; Poeppelmeier, K. R.; Marks, L. D. A Homologous Series of Structures on the Surface of $SrTiO_3$ (110). *Nat. Mater.* **2010**, *9*, 245−248.

DOI: 10.1021/acs.chemmater.7b04404
Chem. Mater. XXXX, XXX, XXX−XXX